Targeting Tumor Vasculature With an Oncolytic Virus

Caroline J Breitbach[1–3], Naomi S De Silva[1,2], Theresa J Falls[1], Usaf Aladl[4], Laura Evgin[2], Jennifer Paterson[1,2], Yang Yang Sun[1], Dominic G Roy[1,2], Julia L Rintoul[1,2], Manijeh Daneshmand[1], Kelley Parato[1], Marianne M Stanford[1], Brian D Lichty[5], Aaron Fenster[4], David Kirn[3], Harold Atkins[1] and John C Bell[1–3]

[1]Centre for Cancer Therapeutics, Ottawa Health Research Institute, Ottawa, Ontario, Canada; [2]Department of Biochemistry, Microbiology and Immunology, University of Ottawa, Ottawa, Ontario, Canada; [3]Jennerex Inc., San Francisco, California, USA; [4]Imaging Research Laboratories, Robarts Research Institute, London, Ontario, Canada; [5]Centre for Gene Therapeutics, Department of Pathology and Molecular Medicine, McMaster University, Hamilton, Ontario, Canada

Oncolytic viruses (OVs) have been engineered or selected for cancer cell-specific infection however, we have found that following intravenous administration of vesicular stomatitis virus (VSV), tumor cell killing rapidly extends far beyond the initial sites of infection. We show here for the first time that VSV directly infects and destroys tumor vasculature *in vivo* but leaves normal vasculature intact. Three-dimensional (3D) reconstruction of infected tumors revealed that the majority of the tumor mass lacks significant blood flow in contrast to uninfected tumors, which exhibit relatively uniform perfusion. VSV replication in tumor neovasculature and spread within the tumor mass, initiates an inflammatory reaction including a neutrophil-dependent initiation of microclots within tumor blood vessels. Within 6 hours of intravenous administration of VSV and continuing for at least 24 hours, we observed the initiation of blood clots within the tumor vasculature whereas normal vasculature remained clot free. Blocking blood clot formation with thrombin inhibitors prevented tumor vascular collapse. Our results demonstrate that the therapeutic activity of an OV can go far beyond simple infection and lysis of malignant cells.

Received 17 June 2010; accepted 27 January 2011; published online 1 March 2011. doi:10.1038/mt.2011.26

INTRODUCTION

The idea of using viruses to attack and destroy cancer cells is gaining momentum as clinical support for the concept continues to mount.[1,2] A variety of clever engineering strategies that lead to selective replication of oncolytic viruses (OVs) in cancer cells have created a remarkably safe therapeutic platform.[3] Although the mechanisms behind restricted virus replication in malignant cells are well established, the complexities of the interplay between the therapeutic virus and the host are still incompletely understood.[4,5] In particular it appears that multiple interactions of the virus with the patient's immune system, blood components, reticuloendothelial system, and the tumor microenvironment all can augment or mitigate the therapeutic efficacy of a particular virus platform.[6] Understanding the mechanism of action of OVs *in vivo* is critical to the design and optimization of therapeutic regimens and combination therapies in future clinical trials as well as optimizing the therapeutic efficacy of the next generation viruses currently in development. Indeed, one key attribute of OV therapeutics is their potential to target the tumor via multiple mechanisms increasing malignant cell killing and decreasing the incidence of therapeutic resistance.[7]

We have been investigating the interaction of OVs with tumor vasculature as this is the key entry point of any systemically administered therapeutic. Attacking the tumor vasculature with a therapeutic virus has some obvious potential advantages as this could lead to destruction of neovasculature, providing a beacon for recruiting the immune system to the infected tumor and of course be an entry point for the virus into the tumor mass.[8] In earlier studies, we have shown that an engineered version of vesicular stomatitis virus (VSV), a prototype OV with activity in a large variety of mouse tumor models, causes catastrophic loss of blood flow in the tumor bed resulting in massive bystander killing of cancer cells following intravenous delivery.[9] This phenomenon was also demonstrated with oncolytic vaccinia virus.[9,10] Furthermore, infection of the tumor resulted in significant increases in the transcription of genes that encode proinflammatory molecules leading to the recruitment of neutrophils and other immune cells to the tumor bed.[9] Here, we have examined the direct interaction of VSV with tumor blood vessels and show for the first time, that limited sites of virus infection of neovasculature correlate with massive cell death within the tumor. We characterized the mechanism behind the massive bystander killing within the infected tumor and found that neutrophil-dependent initiation of microclots within blood vessels led to irreversible damage of tumor vasculature. We demonstrate that intravascular clot formation robustly potentiates the anticancer activity of VSV by reducing proliferation and inducing apoptosis of tumor cells. Most importantly, the infection of vasculature and subsequent initiation of fibrin deposition and clot formation is restricted to tumor beds. Our findings support the idea

The first two authors contributed equally to this work.

Correspondence: *John C Bell, Centre for Cancer Therapeutics, Ottawa Hospital Research Institute, 501 Smyth Road, Ottawa, Ontario K1H 8L6, Canada. E-mail: jbell@ohri.ca*

that OV infection of tumor vasculature and intravascular coagulation are important components of the antitumor activity of VSV.

RESULTS

3D rendering of images of tumor perfusion and virus infection reveals isolated areas of virus infection and a large reduction in tumor perfusion

We have previously shown that VSV infection of tumors causes a rapid reduction of tumor perfusion within 24 hours of treatment. Our initial findings were based upon immunohistochemical analysis of individual tumor sections (**Figure 1a**); however, these provided limited understanding of the virus interactions within the entire tumor. We therefore constructed 3D models of uninfected and VSV-infected CT-26 colon tumors from ~1,000 serial histological sections (example of individual section in **Figure 1a**) per tumor, in order to permit immunohistochemical analysis of virus infection and spread throughout the entire tumor. To gain an understanding of both sites of virus infection and tumor perfusion, fluorescent microspheres were infused intravenously 5 minutes before animal sacrifice and viewed in individual sections by scanning as described previously (**Figure 1b** infected and **1c** uninfected).[9] The immunohistochemically stained sections were digitally scanned and combined with fluorescent images using the *HTK Histology Toolkit* to create a three-dimensional (3D) rendering of the infected tumor (see Materials and Methods section).

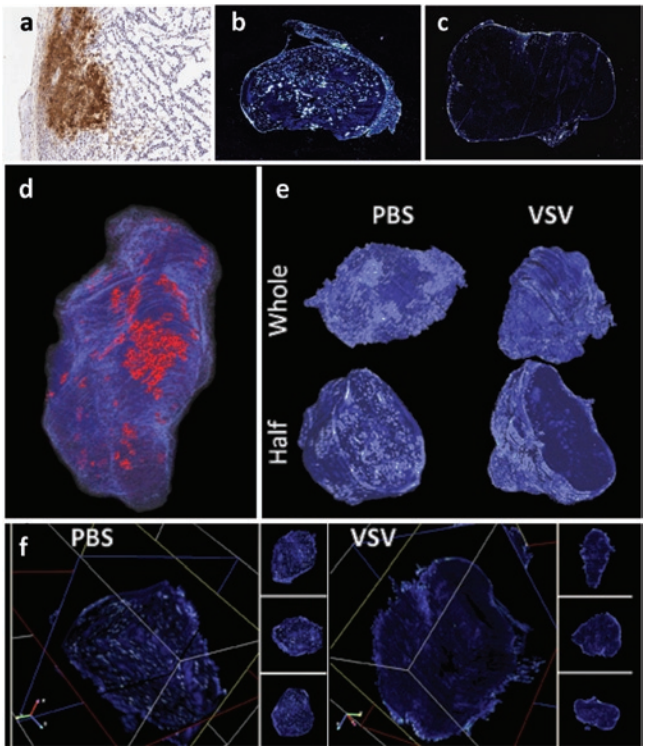

Figure 1 Vesicular stomatitis virus (VSV) infection and tumor perfusion are restricted to the tumor surface. A three-dimensional (3D) tumor model was reconstructed from two-dimensional (2D) digital images of serial histological sections. A CT-26 tumor-bearing BALB/c mouse was treated with VSV for 24 hours and perfused with fluorescent microspheres. (**a**) Serial sections from the excised tumor were stained with antibodies to VSV to visualize sites of virus infection. (**b**) Serial sections of an untreated tumor were then scanned for fluorescent microspheres in order to visualize perfusion. (**c**) A similar analysis of perfusion was generated from serial sections of a VSV-treated tumor. (**d**) Viewing the tumor in *HTK Histology Toolkit* reveals that infection (red) and perfusion (blue) are limited to the tumor surface. Areas of infection are localized to one region of the tumor surface. (**e**) 3D models of tumor perfusion of a VSV-treated tumor and a phosphate-buffered saline (PBS)-treated tumor were reconstructed from images of serial histological sections. Viewing perfusion of whole and half 3D models reveals that the surface of both VSV- and PBS-treated tumors are perfused. Half models show that the tumor core of the VSV-treated tumor is dramatically less perfused when compared to the PBS-treated tumor. (**f**) Using *HTK Histology Toolkit*, scanning through the VSV-treated tumor along x, y, and z axes consistently shows perfusion that is present in the tumor rim but absent from the core. In contrast, visualization of the PBS-treated tumor shows perfusion throughout the tumor.

The 3D visualization of VSV 24 hours postintravenous infusion revealed that VSV (red) infects numerous areas of the tumor but is primarily limited to one major area of the tumor rim (**Figure 1d**) and in **Supplementary Video S1**. Tumor perfusion (light blue) is restricted exclusively to the tumor rim, as best visualized in a cross-section of the tumor (**Figure 1e**) and in **Supplementary Video S2**. Similar rendering of perfusion images of an untreated tumor reveals that CT-26 tumor perfusion is fairly uniform (**Figure 1e** and **Supplementary Video S2**) and provides a stark contrast to the reduction in perfusion triggered by virus infection. In another representation, cross-sections of the untreated and treated tumors in all three orthogonal planes revealed a complete loss of perfusion in the tumor core of the treated tumor with uniform perfusion in the untreated control (**Figure 1f**). By scanning through the entire tumor for each treatment (**Supplementary Video S3**), we observed that this loss of perfusion consistently extends throughout the entire tumor. The 3D rendering of virus infection and tumor perfusion reveals the full scope of the early events caused by OV infection and their impact on tumor physiology.

VSV treatment reduces proliferation of malignant cells within the tumor core

Given the drastic change in tumor perfusion observed over the course of OV therapy, we next investigated the effect of VSV infection on tumor cell proliferation. We monitored proliferation in the same tumor before (by BrdU incorporation) and after (by Ki67 staining) VSV treatment. Twenty-four hours before virus treatment, mice were pulsed with 5′-bromo-2′-deoxyuridine (BrdU), which is incorporated into DNA as it is being synthesized at the time of infusion. Mice were then challenged with VSV and euthanized the following day (**Figure 2a**). In histological sections of untreated tumors, regions of BrdU positive tumor cells (identified pathologically) correlate exactly with Ki67 staining, which marks cells proliferating at the time of mouse euthanasia. However, in tumors taken from mice treated with virus, while BrdU staining is uniform throughout the entire tumor, Ki67 staining is only detected in the tumor rim. Small areas of virus staining were also detected within the tumor rim (**Figure 2b**). Ki67 quantitation in treated versus untreated tumors demonstrated significantly less proliferation after OV therapy (**Figure 2c**). This experiment therefore demonstrates that the extent and distribution of tumor cell proliferation changes drastically over the course of VSV treatment. Decreased cell proliferation is maintained at late timepoints (22 days post-treatment) as observed in representative sections (**Figure 2d**). It is apparent that at both early and late timepoints,

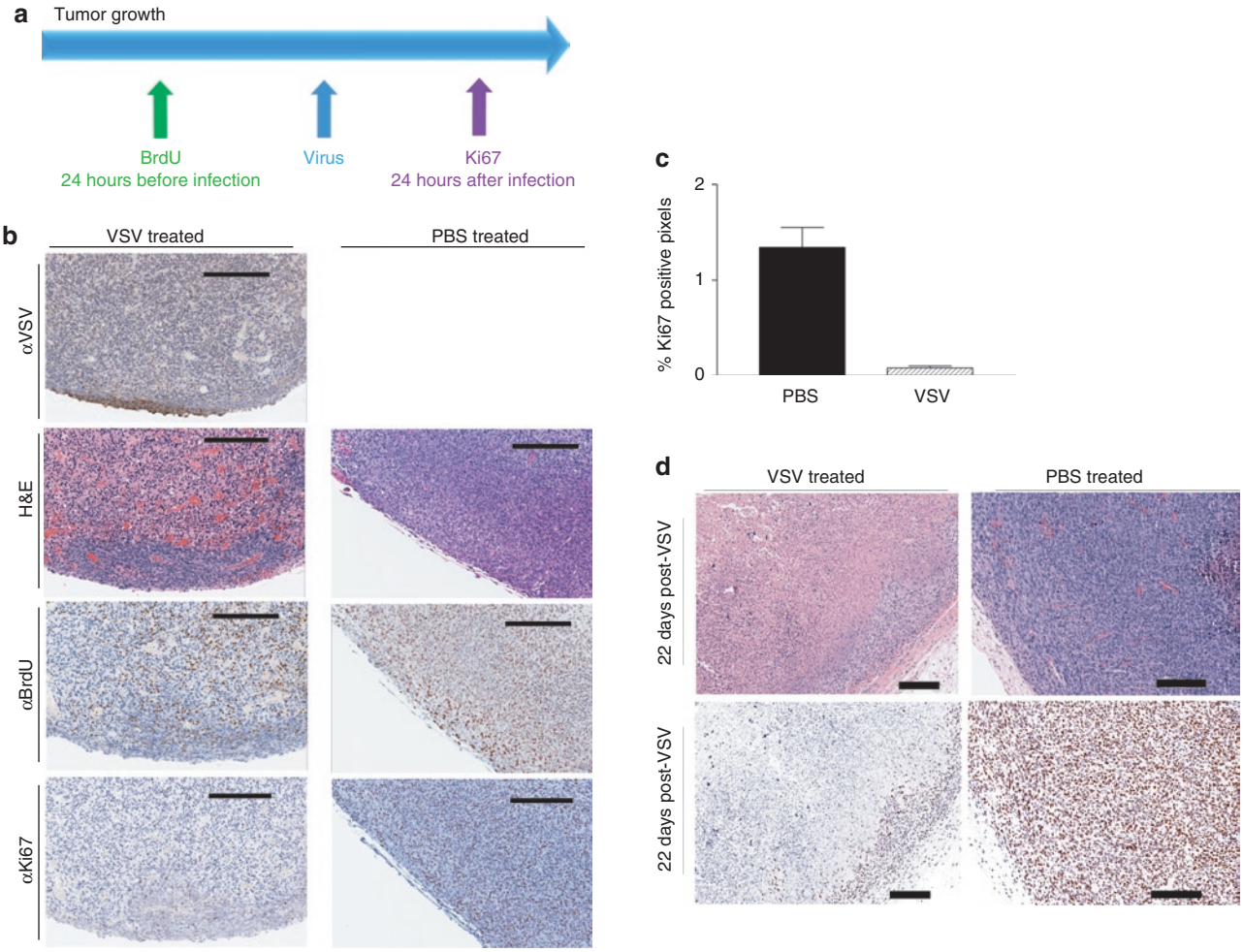

Figure 2 Decreased cell proliferation observed following vesicular stomatitis virus (VSV) treatment. (**a**) Experimental setup. BALB/c mice-bearing subcutaneous CT-26 tumors were pulsed with 5′-bromo-2′-deoxyuridine (BrdU) 24 hours before receiving VSV intravenously (or left untreated). Twenty-four hours following virus challenge, three mice per group were euthanized and tumors were embedded for sectioning. (**b**) Tumor sections were stained for immunohistochemical analysis to detect VSV (virus infection), Ki67 (cell proliferation), and BrdU (proliferating cells that incorporated bromodeoxyuridine). Serial sections were stained with hematoxylin & eosin to visualize tissue architecture. At 24 hours, there is a decreased visualization of Ki67 staining in the VSV-treated tumor. Bar = 200 μm. (**c**) Quantification (mean + SD) of Ki67 staining in VSV-treated versus phosphate-buffered saline (PBS)-treated tumor at 24 hours post-treatment. Quantification of three mice per group was performed using Aperio software. (**d**) By 22 days postinfection, extensive necrosis is evident within the tumor core however, viable tumor cells persist within the tumor rim. It is apparent that Ki67 staining is limited to the tumor rim. Bar = 200 μm. Image contrast was adjusted to 50 in all Ki67 stained images using Adobe Photoshop Version 8.

Ki67 staining is limited to the tumor rim, which is associated with perfused tissue (**Figure 1f**). These observations confirm that the reduction in cell proliferation, though caused by virus infection of tumors, is largely a result of uninfected tumor cell death, we believe triggered by a decrease in tumor perfusion.

OV therapy destroys tumor vasculature

Given the drastic change in tumor perfusion and proliferation observed over the course of OV therapy, we investigated the integrity of tumor vasculature after VSV treatment. Tumors removed from mice treated with replication incompetent UV-inactivated VSV were compared to tumors taken from mice treated with VSV for 15 hours. Sections were prepared and stained with an anti-CD31 antibody to identify vascular endothelial cells. In sections from tumors infected with intravenously administered, UV inactivated VSV, vascular endothelial cells were uniformly distributed throughout the tumor (brown staining **Figure 3**). In contrast, tumors from mice treated with replication competent VSV had substantially fewer blood vessels and these were almost exclusively found in the tumor rim (**Figure 3**). We examined microscopically, five representative fields in both the rim and core of treated and untreated tumors to evaluate the number of CD31 positive vessels. We found a fourfold reduction of CD31 staining in the rim and 137-fold reduction in the core following VSV treatment. The observation that VSV-infected tumors lacked any intact blood vessels in the centre of the tumor but had apparently intact vessels at the rim is consistent with the tumor perfusion observed in our 3D model.

VSV directly infects tumor vasculature

The profound effect that VSV treatment had on both vascular endothelial cell numbers and tumor perfusion suggested that the

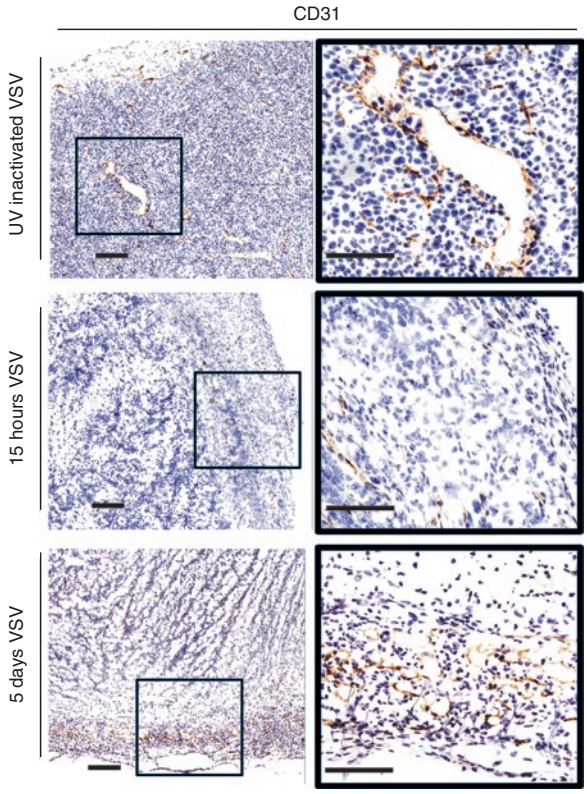

Figure 3 Vesicular stomatitis virus (VSV) treatment results in decreased tumor vasculature. BALB/c mice-bearing CT-26 tumors were treated intravenously with UV-inactivated VSV, or VSV intravenously. Five mice per treatment were euthanized at the indicated timepoints. Tumors were frozen for sectioning. Tumor sections were stained with an antibody detecting CD31, an endothelial cell marker. Endothelial cells are uniformly distributed in control tumors but are restricted to the tumor edge following VSV treatment. Bar = 200 µm. Image contrast was adjusted to 50 in all images using Adobe Photoshop Version 8.

virus was directly infecting neovasculature. Indeed, upon intravenous infusion of VSV, tumor-associated endothelial cells are likely the first cells within the tumor the virus comes in contact with. We therefore first evaluated whole mount tumors following intravenous infusion with a form of VSV that expresses green fluorescent protein (VSV-GFP) in infected cells. Mice were euthanized several hours post-treatment and tumors were evaluated under a fluorescent dissecting microscope. The expression of GFP within infected cells was clearly visible along the length of blood vessels on the surface of the tumor (**Figure 4a**). The GFP signal tracks into the tumor as the virus apparently spreads from the site of initial infection into the tumor. Sections of infected tumors were prepared and examined microscopically. Immunohistochemical analysis of these sections confirmed that VSV is directly infecting tumor vasculature and then subsequently spreading into tumor tissue (**Figure 4b**).

We examined a variety of mouse tissues to determine whether VSV is capable of initiating infections in normal mature vasculature. In treated animals, we were unable to detect VSV-GFP expression in any normal organs (data not shown). We then prepared sections from a variety of normal tissues including skeletal muscle adjacent to the tumor, lung, heart, and brain. In none of these tissues nor the vasculature within them (**Figure 4c**) were we able to detect active VSV replication using immunohistochemical analysis. These results demonstrate that VSV appears unable to initiate infections in normal vascular endothelium but is capable of infecting tumor neovasculature and spreading from these initial sites of infection into the tumor proper.

OV therapy induces clot formation in tumor vasculature

Our 3D model clearly demonstrated that while there were limited sites of infection, the effects on tumor perfusion were quite profound (see **Figure 1**). This suggested that some limited infection of tumor vasculature and adjacent tumor cells leads to occlusion of blood vessels that resulted in a loss of blood flow throughout the tumor. One possible explanation is the virus damaged the neovasculature and this initiated the formation of blood clots within infected vessels. We examined tumor sections using antibodies to fibrin since deposition of this protein is characteristic of clot formation.[11,12] We found that infected tumors had extensive fibrin staining consistent with the idea that VSV infection of CT-26 tumors triggers extensive blood clot formation in tumor blood vessels and areas of hemorrhage (**Figure 5a**). In contrast, uninfected tumors contain unclogged vessels with no detectable fibrin deposits.

As an impressive induction in intravascular blood clot formation was observed in tumors of VSV-treated mice, we wanted to determine whether this phenomenon was restricted to the infected tumor bed. We analyzed hematoxylin & eosin stained sections of brain, lung, heart, and tumor-adjacent skeletal muscle tissue and observed no increase in blood clot formation in these normal tissues taken from treated mice when compared to untreated controls (**Figure 5d**, quantification **Figure 5e**). These results demonstrate the normal tissue vasculature is resistant to VSV-induced clot formation.

Induction of clot formation is followed by decreased tumor proliferation

We observed that intravascular clot formation was absent in vessels located within the perfused, viable tumor rim (data not shown). Furthermore, intravascular clots were present throughout the tumor core and were associated with decreased tumor cell proliferation (**Figure 2**). A likely explanation is that occlusion of microcirculation by intravascular clots may deprive tumor cells of essential nutrients required to drive proliferation. Indeed, in mice treated with virus, we observe that decreased tumor cell proliferation occurs shortly after the induction of clot formation. In a detailed time-course experiment following fibrin clot formation and proliferation, increased blood clot formation was detected starting at 6 hours (**Figure 5b**), which preceded the decrease in proliferation observed as early as 9 hours (**Figure 5c**).

Intratumoral coagulation is dependent on neutrophils

In earlier studies, we demonstrated that virus mediated loss of tumor perfusion was dependent upon the presence of neutrophils.[9] Others have demonstrated that neutrophil recruitment during natural pathological infections of normal tissues, leads to clot formation.[13] In virus-treated tumors, we observed inflammatory

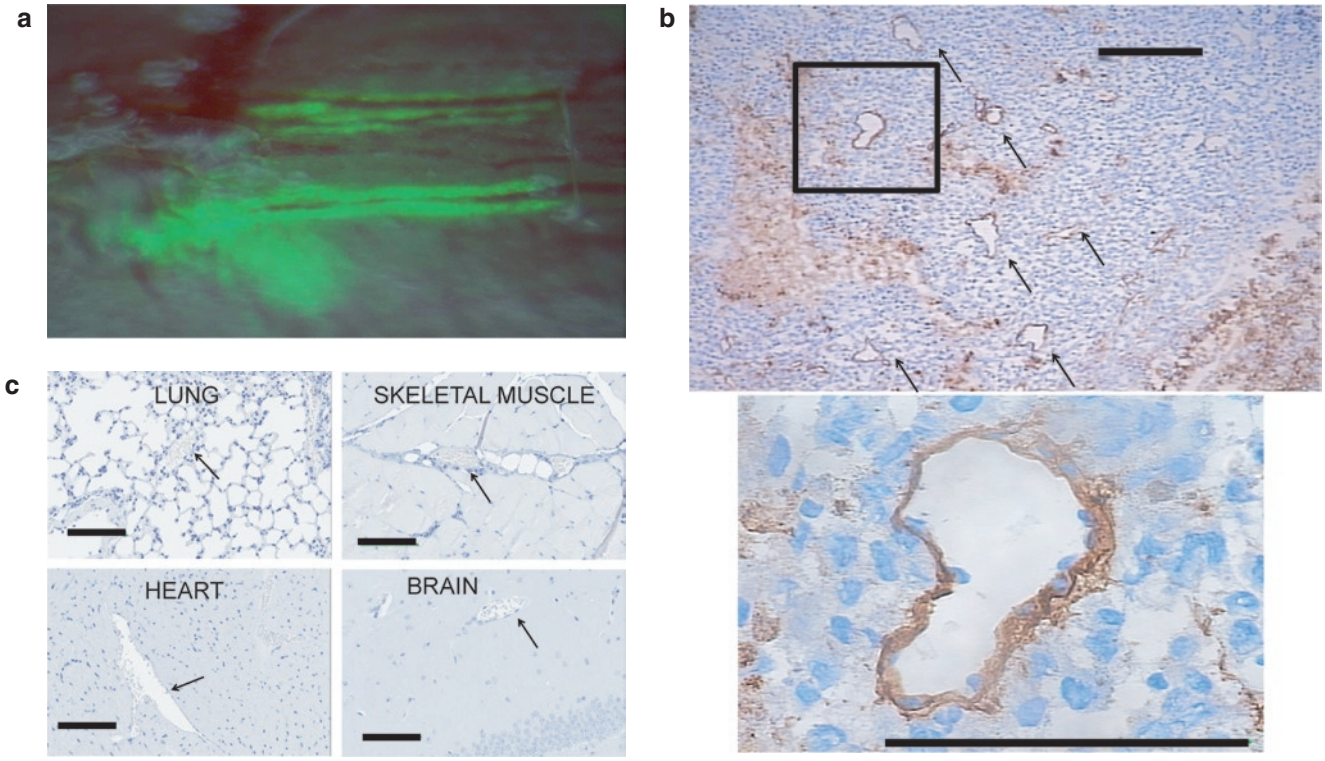

Figure 4 Vesicular stomatitis virus (VSV) infects tumor vasculature. (**a**) CT-26 subcutaneous tumor-bearing BALB/c mice were treated intravenously with VSV-expressing green fluorescent protein (GFP) and euthanized 24 hours later. Dissecting fluorescence microscopy was used to perform *in situ* imaging of tumor. Overlay of bright field and green fluorescence. VSV infection visualized along vessels. (**b**) BALB/c mice-bearing CT-26 tumors were treated intravenously with VSV-expressing GFP and sacrificed 24 hours later. Sections of tumors were stained by immunohistochemistry for VSV antigens. VSV infection is localized to tumor vasculature (black arrows) and surrounding tumor tissue. Bar = 100 µm. (**c**) Brain, lung, heart, and tumor-adjacent skeletal muscle tissue were excised from five tumor-bearing BALB/c mice that were treated intravenously with VSV. No VSV antigen was detected in normal vasculature (arrows) and representative images are shown. Bar = 100 µm.

cells, including neutrophils, at sites of thrombus formation (**Figure 6a**). Suspecting that neutrophils mediate clot formation, which would lead to decreased tumor perfusion, we compared and contrasted infected CT-26 tumors harvested from neutrophil intact or depleted mice for the presence of fibrin clots. To this end, mice were treated with GR-1, an antibody that can be used to deplete neutrophils.[14,15] Under conditions where we observed dramatically reduced concentrations of neutrophils in the blood of treated mice (data not shown), we found that infected tumors had significantly reduced fibrin deposition (**Figure 6b**). These results coupled with our previous observations that neutrophils are required for virus-induced loss of tumor perfusion supports the idea that neutrophils are required for induction of coagulation in tumors treated with OVs. These observations underscore the importance of an inflammatory reaction in triggering coagulation and loss of tumor perfusion during OV therapy.

OV therapy induces intratumoral coagulation triggering a reduction in tumor perfusion

To test whether the presence of fibrin clots is responsible for the loss of blood flow in OV-infected tumors, we attempted to inhibit clot formation during therapy using heparin or bothroalternin, a thrombin inhibitor isolated from snake venom.[16] Groups of three tumor-bearing mice were continuously treated with either thrombin inhibitor in combination with VSV, and we found an even distribution of microspheres throughout the tumor (**Figure 7**) suggesting that formation of microclots within tumor vasculature is responsible for the loss of blood flow we observed during OV therapy. In contrast, mice treated with VSV in conjunction with tissue plasminogen activator, an enzyme that breaks down clots, we observed a loss of perfusion in the tumor core suggesting that once clots are initiated, irreversible vascular destruction ensues. These experiments demonstrate that inflammation triggered by OV infection within tumors activates blood clot formation in tumor microvasculature resulting in a loss of tumor perfusion. This effect can be blocked by continuous treatment with thrombin inhibitors but once initiated causes irreversible damage.

Virus initiated coagulation correlates with increased tumor cell killing

To determine the effect that virus-induced coagulation had on tumor physiology, we compared and contrasted VSV-treated tumor-bearing mice in the presence or absence of heparin. We found that heparin effectively reduced the formation of fibrin clots in response to VSV treatment (**Figure 8**). In heparin-treated tumors there was a coincident increase in Ki67 staining and a decrease in active caspase 3 staining (**Figure 8**). It is known that under some conditions, heparin can affect the ability of certain viruses to infect cells[17] and therefore the reduction of fibrin clots could have simply been a consequence of reduced VSV infection.

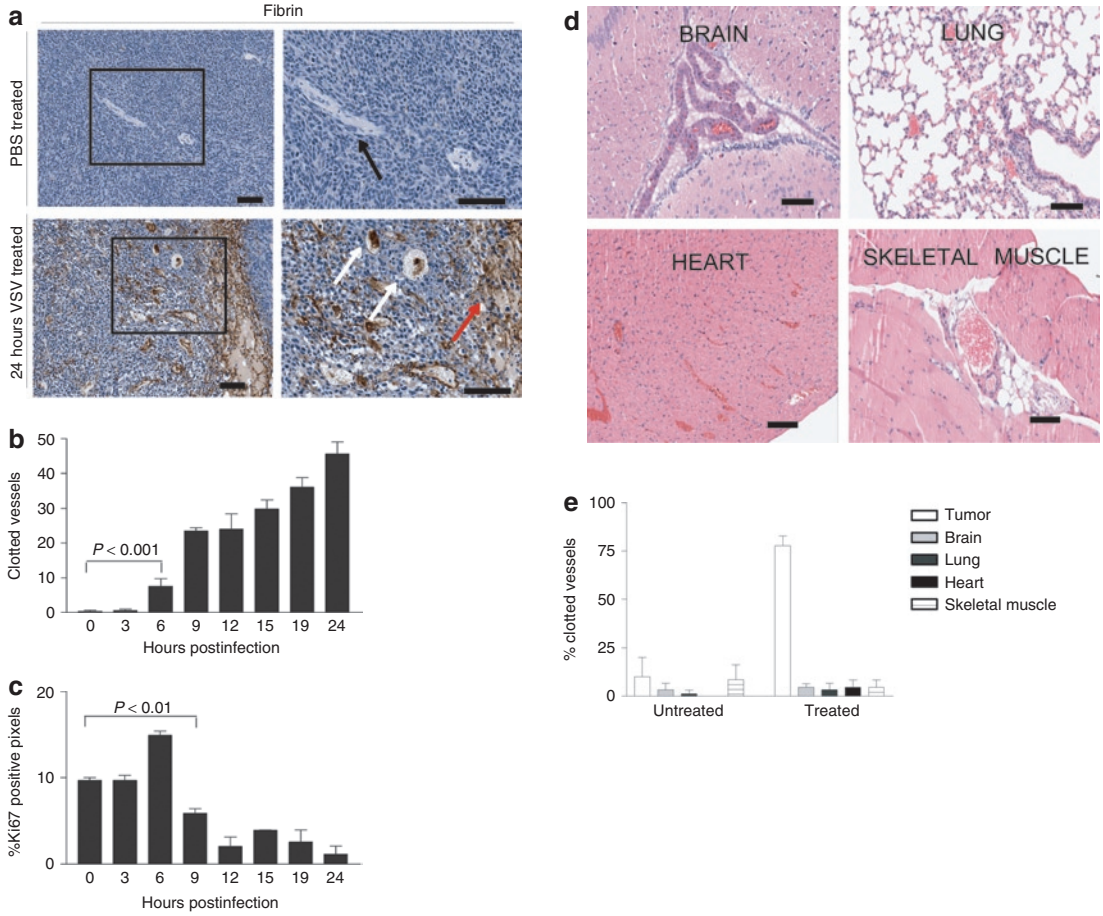

Figure 5 Oncolytic virus infection triggers coagulation within tumor vasculature and tumor cell proliferation decreases shortly after the onset of clot formation. (**a**) BALB/c mice with CT-26 tumors were treated intravenously with vesicular stomatitis virus- (VSV) expressing green fluorescent protein (GFP) and sacrificed at 3 hours postinfection (control) and 24 hours postinfection. Sections were stained with antibody that detects fibrin deposits. Note vessels (black arrows), clogged vessels (white arrows) and areas of hemorrhage (red arrows). Bar = 500 µm, left images; bar = 200 µm, right images. (**b**) Mice were treated with VSV and euthanized at various timepoints postinfection. Tumors were immunohistochemically stained to detect fibrin deposits. Clotted vessels of three tumors per timepoint were counted from five random fields of view per tumor (mean + SEM). Clot formation is initiated as early as 6 hours postinfection. *P* value determined by analysis of variance (ANOVA). (**c**) The same tumors were then stained for Ki67 and positive pixels were quantified and are expressed as percent positive pixels ×10 (mean + SEM). Decreased proliferation is first detected 9 hours post-treatment. (**d**) Vessels associated with normal tissues do not exhibit increased coagulation. Brain, lung, heart, and tumor-adjacent skeletal muscle tissue were excised from tumor-bearing BALB/c mice that were treated intravenously with VSV. Hematoxylin & eosin stained sections of vessels associated with normal tissues are shown. Bar = 100 µm. (**e**) Percentage of clotted vessels were quantified in tumor, brain, lung, heart, and tumor-adjacent skeletal muscle tissue from untreated mice and mice treated intravenously with VSV (mean + SD). Results obtained from five mice per treatment.

Upon examination of infected, heparin-treated tumors we found however no difference in the number of initial sites of VSV infection (identified by immunohistochemical staining). In addition, *in vitro* infections in the presence of heparin did not impact the ability of VSV to infect cells (data not shown). In these experiments, induction of clot formation correlated with potentiated tumor cell killing well beyond the limited sites of infection observed at 24 hours (**Figure 1**).

DISCUSSION

Herein, we describe for the first time, a natural tumor vasculature targeting ability of the OV VSV, which leads to tumor blood vessel coagulation and ultimately vascular collapse. Induction of blood clot formation over time correlated with decreased tumor cell proliferation. This phenomenon can be prevented by treatment with anticoagulants showing that blood clot formation in tumor microvasculature is critical for loss of tumor perfusion. Previously, we demonstrated a critical role for neutrophil recruitment to infected tumor beds that initiates a cascade of events leading to a profound loss of tumor perfusion.[9,18] Our observation that neutrophils are also essential for the initiation of fibrin deposition and clot formation in infected tumors is consistent with a VSV-induced inflammatory reaction at the vascular endothelial surface that profoundly compromises tumor vasculature. As mentioned earlier, neutrophil-initiated coagulation is well known in pathological infections of normal tissues.[19] In particular, a recent study has demonstrated that neutrophil elastase and cathepsin G promote coagulation and intravascular thrombus growth.[20] It appears that OV infection of tumor neovasculature simply initiates a preprogrammed host response to virus infection focusing

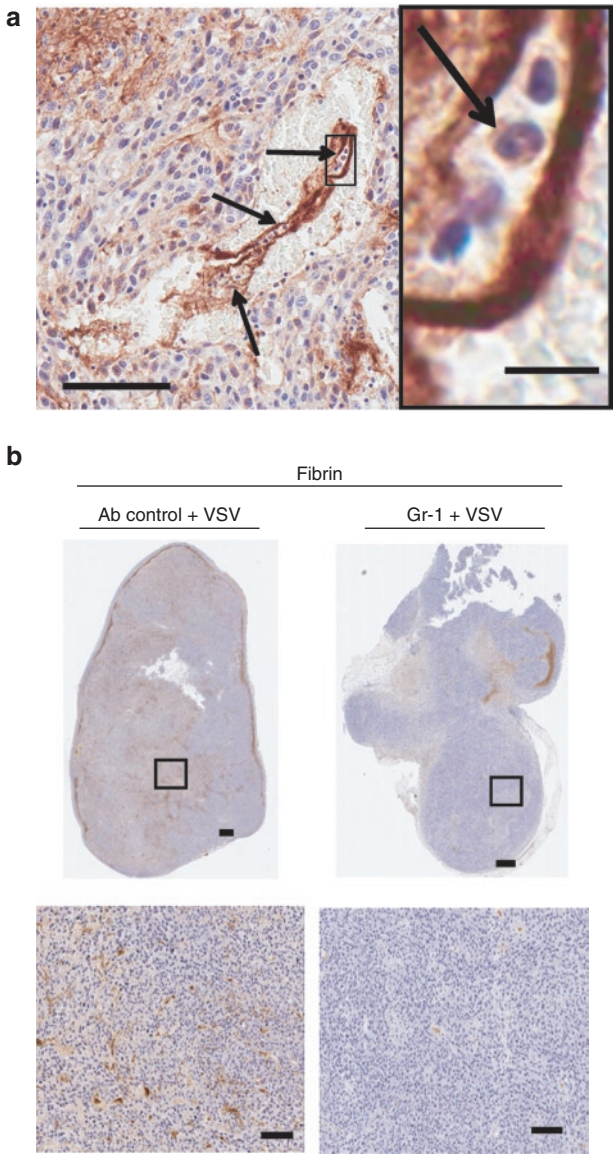

Figure 6 Decreased clot formation is observed in tumors from neutrophil-depleted mice. (**a**) A fibrin clot within a tumor vessel. Arrows indicate neutrophils. Bar = 100 µm, magnification: bar = 10 µm. (**b**) BALB/c mice-bearing CT-26 tumors were pretreated with RB6 8C5 antibody or 50:50 rat serum:phosphate-buffered saline intraperitoneally 24 hours before intravenous treatment with vesicular stomatitis virus (VSV). Twenty-four hours after virus treatment, mice were euthanized and tumors embedded for sectioning. Sections were stained to detect fibrin deposits. Decreased fibrin deposition is detected in tumors taken from neutrophil-depleted mice. Representative section of four mice shown. Bar = 100 µm.

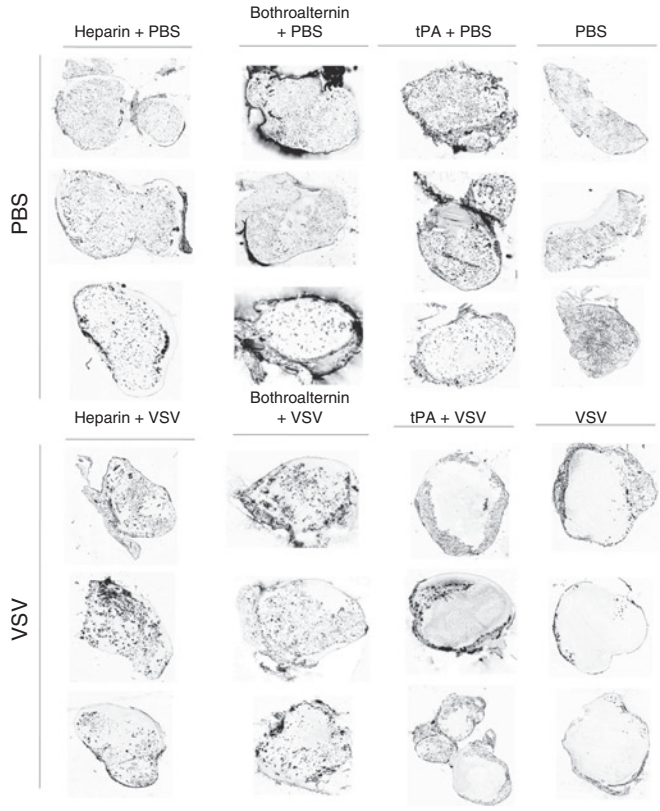

Figure 7 Inhibition of coagulation results in sustained perfusion of oncolytic virus- (OV) treated tumors. BALB/c mice with CT-26 tumors were treated intravenously with phosphate-buffered saline (PBS) or VSV as well as tissue plasminogen activator (tPA), bothroalternin or heparin intraperitoneally. Prior to being sacrificed, mice were perfused with fluorescent microspheres for 5 minutes. Tumor sections were prepared and analyzed for fluorescence using a microarray scanner. Black spots indicate perfused areas. Tumors excised from mice treated with PBS are uniformly perfused. Tumors taken from mice treated with VSV or VSV + tPA demonstrate a loss of tumor perfusion. In contrast, mice treated with thrombin inhibitors bothroalternin or heparin + VSV demonstrate uniform perfusion. Images representative of three mice per treatment are shown.

the normal inflammatory response inside the tumor. This rapid innate host response, whose function in natural infections is to decrease blood flow preventing the spread of pathogens, instead potentiates the anticancer activity of VSV by targeting hypercoagulable tumor vasculature. Indeed our 3D modeling of tumor infection demonstrates that VSV initiates profound tumor killing that would not be predicted from the modest level of tumor infection and virus spread within the tumor. These studies underline the importance of understanding the mechanism of tumor targeting of anticancer agents *in vivo*, in particular with proinflammatory agents like replicating viruses.

The observations presented here have significant implications for the OV field. While we do not currently know that all OVs can infect tumor vasculature, we have shown that this is also a property of oncolytic vaccinia virus.[10] Targeting tumor vasculature has major advantages over only targeting tumor tissue; these include an ease of targeting with IV administration as well as a presumably greater genetic stability of tumor endothelial cells that should decrease the likelihood of evolved resistance to therapeutics that is characteristic of malignant cells. In addition, targeting tumor vasculature may result in "bigger bang for your buck" because as we show here virus targeting of a limited number of endothelial cells can cause broader vascular disruption and significant tumor cell killing. Clinically, the heterogeneity of cancer often poses barriers to direct infection and cell killing by OVs. For example, virus-resistant subpopulations, stromal components, and extracellular matrix are able to prevent efficient infection and spread, thereby limiting the ability of OVs to directly infect and kill malignant

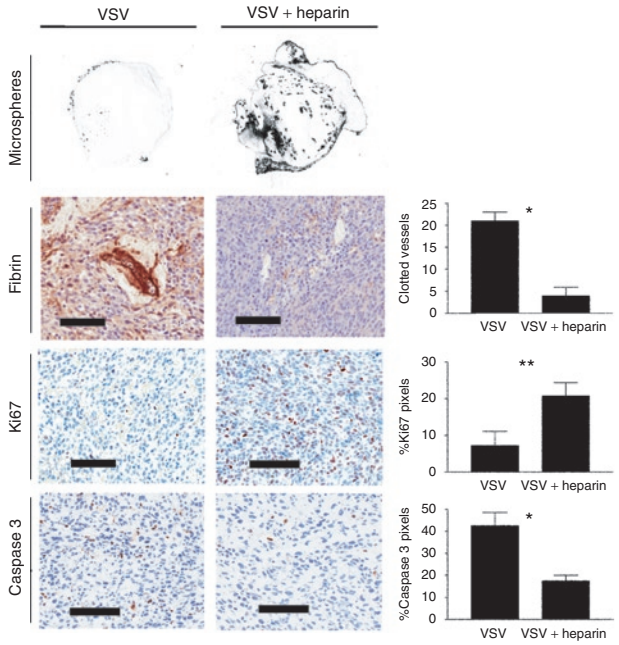

Figure 8 Clot formation results in reduced proliferation and increased apoptosis in oncolytic virus (OV)-treated tumors. BALB/c mice with CT-26 tumors were treated intravenously with either vesicular stomatitis virus (VSV) alone or with heparin in order to inhibit VSV-induced coagulation. Representative histological images are shown with corresponding quantification from four mice per group. Clot formation was quantified as described previously. The same tumors were stained for Ki67 and the active form of caspase 3, markers of proliferation, and apoptosis, respectively. Virus-treated, clotted tumors exhibited less proliferation and more apoptosis relative to tumors treated with VSV and heparin. Staining is expressed as percent positive pixels ×10 (mean + SEM). $*P < 0.005$, $**P < 0.05$.

cells. The ability of OV's to target tumor vasculature provides a mechanism to achieve tumor cell killing while circumventing the need for efficient virus spread throughout the tumor mass.

We clearly demonstrate here for the first time that VSV is able to productively infect tumor neovasculature *in vivo*, but that vascular endothelium in normal tissues is resistant to virus infection. The mechanism of VSV selectivity is not known but recently Vile and colleagues have shown that *in vitro* treatment of human vascular endothelial cells with vascular endothelial growth factor can transiently sensitize these normal cells to infection by reovirus and VSV.[8] It may be that in the tumor microenvironment where blood vessels are being constantly remodeled as a consequence of stimulation by vascular endothelial growth factor and other proangiogenic factors, that vascular endothelium becomes prone to OV infection and destruction. Interestingly, Orf a parapoxvirus encodes a viral form of vascular endothelial growth factor that is known to enhance its pathogenic effects.[21] Perhaps vascular endothelial growth factor stimulation of vascular endothelial cells inhibits or dampens the innate antiviral programs of these cells making them transiently sensitive to virus infection.

Finally, our observation of tumor vascular shutdown in preclinical models led us to investigate changes in tumor perfusion in patients treated with OVs as part of clinical trials. A profound reduction in tumor perfusion was observed in some patients with advanced hepatocellular carcinoma following treatment with an oncolytic poxvirus, JX-594 in early phase trials.[22,23] Clearly, acute vascular disruption of tumors causes decreased tumor cell viability and is therefore an additional mechanism of action of OVs.[9,18] Understanding the mechanism by which OV infection targets tumor vasculature will allow for the development of strategies to exaggerate the effect and increase acute tumor cell killing.[7,24]

MATERIALS AND METHODS

Viruses. The Indiana serotype of VSV was used throughout this study and was propagated in Vero cells (American Type Culture Collection, Burlington, Ontario, Canada). AV1 VSV is a naturally occurring interferon-inducing mutant of VSV[4] while Δ51 VSV-expressing GFP[4] is a recombinant interferon-inducing mutant of the HR strain of wild-type VSV Indiana. TP3, herein referred to as AV2, was inactivated by UV light. Virions were purified from cell culture supernatants by passage through a 0.2 µmol/l Steritop filter (Millipore, Billerica, MA) and centrifugation at 30,000*g* before resuspension in phosphate-buffered saline (PBS) (HyClone, Logan, UT).

Cell lines. CT-26- (murine colon adenocarcinoma) derived cells were purchased from American Type Culture Collection and cultured in HyQ Dulbecco's modified Eagle's medium (high glucose) (HyClone) supplemented with 10% fetal calf serum (CanSera, Etobicoke, Ontario, Canada).

Tumor models. Six to eight-week-old female BALB/c mice were obtained from Charles River Laboratories (Wilmington, MA). Syngeneic subcutaneous tumors were established by injection of 3×10^5 cells in 100-µl PBS (CT-26) in the left and right hind flanks. When tumors reached a palpable size, mice were treated with VSV by tail vein injection. Mice were euthanized at the indicated timepoints by cervical dislocation and on portion of tumors were frozen in Shandon Cryomatrix freezing medium (ThermoElectron, Waltham, MA) on dry ice. Five or ten µmol/l sections were cut using a Microm HM500 OM cryostat (Microm, Walldorf, Germany). Another portion of tumors was placed in 10% formalin and embedded in paraffin. For some experiments, brain, lung, heart, and tumor adjacent skeletal muscle tissue were also collected and paraffin embedded for histological analysis. Mice were not perfused before organ collection. All experiments were conducted with the approval of the University of Ottawa Animal Care and Veterinary Service.

Histological and immunohistochemical analysis. Immunohistochemistry detecting fibrinogen (1:500; DAKO, Glostrup, Denmark) was performed on paraffin-embedded sections using the Vectastain ABC kit for rabbit primary antibodies (Vector Labs, Burlingame, CA), according to instructions provided. The antigen retrieval step was omitted. For Ki67 detection, paraffin-embedded sections were boiled in 10 mmol/l citrate buffer, pH 6. Primary anti-Ki67 antibody (1:25 dilution; DAKO) was applied overnight and detected using anti-rat antibody detection system (DAKO). BrdU was detected using the Vectastain ABC kit for rat primary antibodies (Vector Labs), on paraffin-embedded sections treated with 4 N HCl. Primary anti-BrdU (1:100 dilution; Abcam, Cambridge, MA) was applied for an hour. Horseradish peroxidase activity was visualized with a Diaminobenzene-Horseradish peroxidase kit (KPL Biosciences, Guelph, Canada). Apoptotic cells were detected with a rabbit primary antibody against the active form of Caspase 3 (BD Biosciences, Mississauga, Ontario, Canada) at a dilution of 1:500 using the Vectastain system. Nuclei were counterstained in hematoxylin. For assessment of cell morphology, sections were stained with hematoxylin and eosin according to standard protocols. Staining was digitized using Aperio ScanScope (Axiovision Technologies, Toronta, Ontario, Canada) and analyzed using Aperio ImageScope software. Blood clots in normal tissues of **Figure 6d** were quantified on hematoxylin & eosin stained sections. Thirty vessels were counted per section.

Analysis of tumor perfusion. Mice were injected intravenously with 100 µl of a 50% solution of 100 nm diameter orange fluorescent microspheres

(Molecular Probes, Burlington, Ontario, Canada). Five minutes later, animals were euthanized and tumors immediately snap frozen as previously described. Tumor perfusion was analyzed by visualizing fluorescent microspheres in the vasculature of 10 µm unfixed frozen sections using a ScanArray Express microarray scanner with a standard Cy3 laser (Packard Bioscience, Meriden, CI).

3D modeling of tumor vascularity during OV therapy. CT-26 tumor-bearing mice were treated with VSV or PBS and euthanized 24 hours later. Microspheres were injected as described above and the tumor was collected and frozen. The tumor was cut into 1,085 6-µm tissue sections and mounted on slides. Every fifth section was scanned for microspheres and immunohistochemically stained for VSV as described above. The sections were stained for VSV using the Autostainer Plus (DakoCytomation, Burlington, Ontario, Canada). *HTK Histology Toolkit* software (Robarts Imaging Institute, University of Western Ontario, London, Ontario, Canada) was used to convert 2D images into 3D models. Volume reconstruction was completed using alignment and segmentation contouring algorithms, which oriented each tissue section on top of one another. Each tissue section image, once oriented, was then converted from 2D pixels into 3D voxels. These 3D stacks were then rendered to generate the reconstructed tumor. 2D images of microspheres were used to generate a model of perfusion, while 2D images of VSV staining were used to generate a model of infection. An overlay model was generated from superimposed images of microspheres and VSV. Regions of infection were highlighted in red to aid in visualization (Adobe Photoshop CS2).

BrdU pulse. Tumor-bearing mice were treated with 100 mg/kg BrdU (Sigma, Oakville, ON) intraperitoneally 24 hours before, or 22 hours after, intravenous injection of VSV or PBS. Twenty-four hours following virus challenge, three mice per group were euthanized and tumors removed, paraffin-embedded and analyzed by immunohistochemistry as described above.

In vivo *neutrophil depletion.* Mice were injected intraperitoneally with 150 µg purified RB6 8C5 rat monoclonal antibody, clone RB6-8C5 (BD Pharmingen, Rockville, MD) in order to systemically deplete granulocytes. One hundred and fifty micro liter of nonimmune rat serum was used as a negative control. Twenty-four hours later, mice were treated intravenously with 5×10^8 plaque-forming unit Δ51 VSV-GFP, perfused with fluorescent microspheres 24 hours later and sacrificed by cervical dislocation and tissues collected and stained as described above.

Manipulation of blood clot formation. Tumor-bearing mice were treated with VSV or PBS intravenously and 200 U/kg heparin [dalteparin sodium injection (Fragmin), Pfizer, New York, NY], intraperitoneally four times over the course of 24 hours starting at the time of VSV injection and ending at 22 hours when the mouse was euthanized. Bothroalternin (Cedarlane, Burlington, ON) or tissue plasminogen activator (Activase rt-PA; Roche, Basel, Switzerland) were injected at 20 U/kg and 4 mg/kg, respectively, intraperitoneally 1 hour before intravenous VSV or PBS infusion and another three times over the course of 21 hours before euthanizing the mice. Effects of coagulation on tumor viability were similarly analyzed 10 hours after virus treatment with administration of 100 U heparin (unfractionated heparin 1,000 USP U/ml; Pharmaceutical Partners of Canada, Richmond Hill, Ontario, Canada) every 2 hours subcutaneously during treatment. In all experiments, mice were injected intravenously with fluorescent microspheres before sacrifice in order to visualize tumor perfusion.

Statistical analysis. All statistical analysis was performed using Graphpad Prism 3.0 software. Data are represented as a mean ± SE. Analysis of variance was performed with Tukey's *post-hoc* test.

SUPPLEMENTARY MATERIAL

Video S1. 3D model of VSV infection and perfusion.

Video S2. Cross-sections of perfusion models of VSV- and PBS-treated tumors.

Video S3. Scan throughs of VSV and PBS perfusion models.

ACKNOWLEDGMENTS

This work was supported by grants to J.C.B. from the Terry Fox Foundation and the Canadian Institute for Health Research (CIHR). N.S.D. was supported by a Vanier Canada Graduate Scholarship. C.J.B. was supported by an NSERC studentship. L.E. was supported by OGSST. J.L.R. was supported by CIHR. B.D.L., A.F., and J.C.B. are supported by Ontario Institute for Cancer Research.

REFERENCES

1. Parato, KA, Senger, D, Forsyth, PA and Bell, JC (2005). Recent progress in the battle between oncolytic viruses and tumours. *Nat Rev Cancer* **5**: 965–976.
2. Cattaneo, R, Miest, T, Shashkova, EV and Barry, MA (2008). Reprogrammed viruses as cancer therapeutics: targeted, armed and shielded. *Nat Rev Microbiol* **6**: 529–540.
3. Bell, JC, Lichty, B and Stojdl, D (2003). Getting oncolytic virus therapies off the ground. *Cancer Cell* **4**: 7–11.
4. Prestwich, RJ, Harrington, KJ, Pandha, HS, Vile, RG, Melcher, AA and Errington, F (2008). Oncolytic viruses: a novel form of immunotherapy. *Expert Rev Anticancer Ther* **8**: 1581–1588.
5. Liu, TC, Galanis, E and Kirn, D (2007). Clinical trial results with oncolytic virotherapy: a century of promise, a decade of progress. *Nat Clin Pract Oncol* **4**: 101–117.
6. De Silva, N, Atkins, H, Kirn, DH, Bell, JC and Breitbach, CJ (2010). Double trouble for tumours: exploiting the tumour microenvironment to enhance anticancer effect of oncolytic viruses. *Cytokine Growth Factor Rev* **21**: 135–141.
7. Kirn, DH and Thorne, SH (2009). Targeted and armed oncolytic poxviruses: a novel multi-mechanistic therapeutic class for cancer. *Nat Rev Cancer* **9**: 64–71.
8. Kottke, T, Hall, G, Pulido, J, Diaz, RM, Thompson, J, Chong, H *et al.* (2010). Antiangiogenic cancer therapy combined with oncolytic virotherapy leads to regression of established tumors in mice. *J Clin Invest* **120**: 1551–1560.
9. Breitbach, CJ, Paterson, JM, Lemay, CG, Falls, TJ, McGuire, A, Parato, KA *et al.* (2007). Targeted inflammation during oncolytic virus therapy severely compromises tumor blood flow. *Mol Ther* **15**: 1686–1693.
10. Kirn, DH, Wang, Y, Le Boeuf, F, Bell, J and Thorne, SH (2007). Targeting of interferon-beta to produce a specific, multi-mechanistic oncolytic vaccinia virus. *PLoS Med* **4**: e353.
11. Corral, J, Yélamos, J, Hernández-Espinosa, D, Monreal, Y, Mota, R, Arcas, I *et al.* (2005). Role of lipopolysaccharide and cecal ligation and puncture on blood coagulation and inflammation in sensitive and resistant mice models. *Am J Pathol* **166**: 1089–1098.
12. Chen, D, Giannopoulos, K, Shiels, PG, Webster, Z, McVey, JH, Kemball-Cook, G *et al.* (2004). Inhibition of intravascular thrombosis in murine endotoxemia by targeted expression of hirudin and tissue factor pathway inhibitor analogs to activated endothelium. *Blood* **104**: 1344–1349.
13. Luscinskas FW (2001). Cytokines and endothelial cell activation. In: Ley, K (ed.). *Physiology of Inflammation*. Oxford University Press: New York, pp 80–89.
14. Maus, U, von Grote, K, Kuziel, WA, Mack, M, Miller, EJ, Cihak, J *et al.* (2002). The role of CC chemokine receptor 2 in alveolar monocyte and neutrophil immigration in intact mice. *Am J Respir Crit Care Med* **166**: 268–273.
15. Tepper, RI, Coffman, RL and Leder, P (1992). An eosinophil-dependent mechanism for the antitumor effect of interleukin-4. *Science* **257**: 548–551.
16. Castro, HC, Dutra, DL, Oliveira-Carvalho, AL and Zingali, RB (1998). Bothroalternin, a thrombin inhibitor from the venom of Bothrops alternatus. *Toxicon* **36**: 1903–1912.
17. Baba, M, Snoeck, R, Pauwels, R and de Clercq, E (1988). Sulfated polysaccharides are potent and selective inhibitors of various enveloped viruses, including herpes simplex virus, cytomegalovirus, vesicular stomatitis virus, and human immunodeficiency virus. *Antimicrob Agents Chemother* **32**: 1742–1745.
18. Varani, J and Ward, PA (1994). Mechanisms of endothelial cell injury in acute inflammation. *Shock* **2**: 311–319.
19. Westlin, WF and Gimbrone, MA Jr (1993). Neutrophil-mediated damage to human vascular endothelium. Role of cytokine activation. *Am J Pathol* **142**: 117–128.
20. Massberg, S, Grahl, L, von Bruehl, ML, Manukyan, D, Pfeiler, S, Goosmann, C *et al.* (2010). Reciprocal coupling of coagulation and innate immunity via neutrophil serine proteases. *Nat Med* **16**: 887–896.
21. Savory, LJ, Stacker, SA, Fleming, SB, Niven, BE and Mercer, AA (2000). Viral vascular endothelial growth factor plays a critical role in orf virus infection. *J Virol* **74**: 10699–10706.
22. Liu, TC, Hwang, T, Park, BH, Bell, J and Kirn, DH (2008). The targeted oncolytic poxvirus JX-594 demonstrates antitumoral, antivascular, and anti-HBV activities in patients with hepatocellular carcinoma. *Mol Ther* **16**: 1637–1642.
23. Park, BH, Hwang, T, Liu, TC, Sze, DY, Kim, JS, Kwon, HC *et al.* (2008). Use of a targeted oncolytic poxvirus, JX-594, in patients with refractory primary or metastatic liver cancer: a phase I trial. *Lancet Oncol* **9**: 533–542.
24. Stanford, MM, Breitbach, CJ, Bell, JC and McFadden, G (2008). Innate immunity, tumor microenvironment and oncolytic virus therapy: friends or foes? *Curr Opin Mol Ther* **10**: 32–37.